Ultraviolet Spectroscopy of Planetary Nebulae: Cosmological Implications

T·H·E
OHIO STATE UNIVERSITY

Gary J. Ferland
Department of Astronomy

October 1990

Ultraviolet Spectroscopy of Planetary Nebulae: Cosmological Implications

Gary J. Ferland
Department of Astronomy

October 1990

Semi-Annual Report;

Grant NAG 5 1027

G.J. Ferland, PI

This is the semi-annual report for NASA grant NAG 5 1027. The project goal is to obtain and reduce IUE data on a target of opportunity basis, of classical novae during eruption. These explosions cannot be predicted in advance, and the scheduling flexibility of the IUE satellite is necessary if meaningful data are to be obtained. There have been two well studied nova explosions during the course of the current grant. The first occurred during 1984 (PW Vul) and was well observed with IUE. Even better data were obtained in the later explosion of NQ Vul.

All satellite data have now been reduced by OSU graduate student Pedro Saizar, who is using the data in his Phd research, and who is supported by the current grant. A primary goal in the analysis of the data is to determine the chemical composition of the ejected gas. A second is to better understand the energy source for the explosion, and to determine what powers the ejecta as it leaves the binary star. A paper (attached) has been completed and accepted for publication in the Astrophysical Journal on the first set of observations (PW Vul). These show that the ejecta have a nearly normal composition, unlike other historical novae. They also show that the infrared, optical, and ultraviolet continuum originates in very hot gas (with a temperature between one and ten million degrees Kelvin), and that emission from this very hot gas may be the agent producing ionization in the "nebular" gas, the relatively cool gas producing optical emission.

The second data set (on the nova NQ Vul) have now been reduced, and the results of the investigation are being written up, and will be submitted for publication within the next few months. This paper will discuss the chemical composition of the ejected shell, and draw comparisons between this nova and other examples. Latter papers will go in greater detail into questions concerning the origin of the very hot gas present in the nova explosion, the origin of the x-ray continua usually seen, and how this explosion affects the high energy radiation field of the galaxy. Computer simulations using the Cray Y-MP at the Ohio Supercomputer Center (OSC) are being used to model and better understand the satellite data. These resources are provided *gratis* to the current grant by the OSC. It is expected that the analysis and modelling of the data will be complete, and all results submitted for publication, by the time Mr. Saizar completes his Phd research in roughly 14 months.

PW Vul: A Nova with Nearly Solar Abundances

Pedro Saizar

Department of Astronomy, The Ohio State University

Sumner Starrfield

Department of Physics and Astronomy, Arizona State University

Gary J. Ferland and R. Mark Wagner

Department of Astronomy, The Ohio State University

James W. Truran

Department of Astronomy, University of Illinois, Urbana

Scott J. Kenyon

Smithsonian Astrophysical Laboratory

Warren M. Sparks

Applied Theoretical Physics Division, Los Alamos National Laboratory

Robert E. Williams

Cerro Tololo Inter-American Observatory, National Optical Astronomy

Observatories[1]

and

L. L. Stryker

Department of Physics and Astronomy, Arizona State University

Abstract

Optical spectrophotometry of PW Vulpeculae (Nova Vul 1984 #1) is combined with ultraviolet data to estimate electron temperatures, densities and abundances in the ejecta of this slow classical nova. We also discuss the reddening, the distance, and the evolution of the ultraviolet spectrum.

Abundances are nearly solar, with the exception of Nitrogen, which is substantially higher. Although Neon has been reported to be enhanced in several novae, it does not seem to be the case for PW Vul. We present photoionization model calculations of the ejecta that give a reasonable match of the observed emission spectrum.

A strong featureless continuum, shows that very hot, presumably shock heated, gas plays a major role in determining the energetics of this nova. Emission from this hot gas is responsible for the ionization of the nebular gas. A calculation of the masses of both the hot coronal gas and the cooler nebular gas shows that the former may account for most of the mass of the ejecta.

Subject headings: stars: abundances – stars: individual – stars: novae

I Introduction

It is generally believed that a classical nova outburst originates from a thermonuclear runaway in the surface layers of the white dwarf component of a close binary star. In this picture, the secondary star (usually a red dwarf), has filled its Roche lobe and transfers matter to the white dwarf, which accretes it through a disk. The deposition of hydrogen-rich material onto the surface of a carbon-oxygen or oxygen-neon-magnesium white dwarf will eventually lead to a thermonuclear runaway. The details of the transfer and accretion mechanisms are discussed, for example, by Starrfield (1988), and Shara (1989).

The system abruptly increases in brightness as the outer layers expand following the runaway. As a result of the mixing of core material in the white dwarf's atmosphere, the ejecta will be rich in C, N, O, and Ne. In fact, thermonuclear runaway simulations show that the energetics of the outburst is sensitive, among other parameters, to the abundance of these elements. The ejecta must hit the outer layers of the secondary star and the accretion disk, thus developing a shock. Therefore, the resulting ejecta can be expected to be a combination of original material from the white dwarf as well as gas lost from the companion star. The latter seems likely to have nearly solar abundances.

In this paper we will be concerned with the late developement of the outburst of PW Vulpeculae (Nova Vul 1984 #1). This is a very slow nova with a possible orbital period of about 0.21 days (Hacke 1987). An optical spectroscopic study of this object was done by Kenyon and Wade (1986), the infrared portion was considered by Gehrz *et al.* (1988) and the present paper can be considered as a continuation of their work, including new ultraviolet observations from the *International Ultraviolet Explorer*.

Recent work (Grasdalen and Joyce 1980, Ferland, Lambert, and Woodman 1986, Greenhouse *et al.* 1989) makes it clear that, despite the few optical signatures present, a "coronal line" region plays a major role in the decline. In the following, we will interpret the spectrum in terms of emission from two thermal phases of gas. The "nebular" phase has a temperature of $\sim 10^4 \, K$, and produces the strong optical-ultraviolet emission lines characteristic of declining novae. This emission line spectrum will be used to evaluate the physical conditions and abundances in the ejecta (e.g., Ferland and Shields 1978). The "coronal" phase has a much higher temperature ($T \sim 10^6 \, K$), and weaker line emission, but is the dominant contributor to the optical continuum. We show below that the coronal phase dominates the energetics of the fading nova.

A review of the outburst is presented in the next section. In section III, we obtain independent estimates of the reddening and the distance to the nova. The obsevational material is presented in Section IV. The physical conditions for both the nebular and the coronal line regions are calculated in sections V and VI, respectively. In section VII, we construct a model of the ejecta that gives a reasonable match of the observed spectrum and a final summary is included in section VIII.

II The Outburst

PW Vul reached its maximum visual brightness of 6.3 mag on August 4, 1984 (J.D. 2,445,918). A light curve covering observations made on a period of over 800 days has been published by Gehrz *et al.* (1988). We adopt July 29, 1984, as day 1 of the outburst.

The early optical development was discussed by Kenyon and Wade (1986),

whereas the infrared evolution was discussed by Gehrz et al. (1988). A picture of the outburst can now be presented based on the available data. An optically thick pseudophotosphere expanded during the first 8 days of the outburst. An infrared spectrum at the time of maximum light presented by Gehrz et al. indicates a blackbody temperature of about 6700 K for the material. The slow decline was somewhat irregular. The nova fell by 2 mag. in a period of a few days and showed a slight brightening to 7.3 mag by August 19 (Sowell, Laird, and Thorstensen, 1985). From the light curve we also see that the timescale to fall 3 mag. is $t_3 \sim 140$ days. After the time of maximum light, the ejecta became an optically thin shell both in visible and infrared light. From the width of Hβ, we infer an expansion velocity of about 600 km/sec. This agrees well with Kenyon and Wade's (1986) measurement of the FWHM of Hα.

Ionized gas in the "principal" ejecta was moving at a somewhat slower rate. A spectrum taken in March 27, 1987 with the Perkins 1.8-m telescope is shown in Fig. 1f. The double peak observed in the $[O\,III]\,\lambda5007$ line implies an expansion velocity of about 400 km/sec, and a double Gaussian fit gives 350 ± 40 km/sec. Infrared observations (cf. Gehrz et al. 1988) also suggest ejection velocities of 300-400 km/sec during this phase of the decline.

Gehrz et al. also presented flux measurements of the infrared continuum, which we will supplement with ultraviolet data. Up to day ~ 100, the entire continuum had an energy distribution characteristic of optically thin free-free emission (i.e., $f_\nu \sim const.$). At about day 280, a flux excess developed in the infrared, which they interpret as thermal emission from optically thin dust.

Many novae show evidence for a large component of very hot gas (Grasdalen and Joyce 1980, Ferland, Lambert, and Woodman 1986, Greenhouse et al. 1989).

The bremsstrahlung originating in this region is the main contributor to the optical continuum, and may be responsible for the ionization observed during the nebular phase of the outburst (Grasdalen and Joyce, 1980). We will discuss this further in the following sections.

III Reddening and Distance

An estimate of the reddening can be obtained by using the ratio of intensities of $HeII\lambda1640$ relative to $HeII\lambda4686$. Seaton (1978) calculated the intensities of several Case-B He II recombination lines, including several radiative and collissional processes. He predicted that $j(He\,II\,1640)/j(He\,II\,4686) = 6.81$, for an electron density of $N_e = 10^6\,cm^{-3}$, and a temperature of 10,000 K, which is within the range of observed values as we will show below. The observed ratios for several dates can be computed from the data presented in Tables 3 and 4. This ratio is a weak function of temperature and density, so we assume that it was constant over our observations. Thus, we can derive an $E(B-V)$ for each day, following the method described by Seaton (1979). For days 253, 331, 340, and 681, the $B-V$ excesses are 0.55, 0.71, 0.62, and 0.52, respectively. Therefore, $<E(B-V)>= 0.60 \pm 0.06$.

The color excess just derived is somewhat higher than the one adopted by Duerbeck *et al.* (1984), based on the study of the galactic extinction by Neckel and Klare (1980), who assumed $E(B-V) \sim 0.45$, in the direction to the nova and, thus, a visual absorption of 1.4 mag. To facilitate comparison with other published work, and to check the sensitivity of our results, we will use both values of the color excess in computing the physical conditions in the ejecta.

Duerbeck *et al.* (1984) obtained a distance to the nova of 1.2 kpc, based on

the equivalent width of the interstellar Ca II K line. On the other hand, Gehrz *et al.* (1988), derived a distance of 6.35 ± 0.35 kpc from the angular expansion rate of the pseudophotosphere, and from several estimates of the luminosity from the decline of the light curve. They assumed that the absorption was negligible.

We can obtain an independent estimate of the distance by measuring the amount of reddening in field stars within 3 degrees of the nova, following the method discussed by Schild (1976). The advantadge of this method is that it is independent of the somewhat uncertain properties of the nova. For this purpose, we used the latest version of the *uvby,β* photometric catalogue by Hauck and Mermilliod (1985), kindly provided by the Astronomical Data Center.

The indices c_1 and m_1 can be corrected for absorption using the formulas (Strömgren, 1966),

$$[c_1] = c_1 - 0.20 \cdot (b - y)$$
$$[m_1] = m_1 + 0.18 \cdot (b - y)$$

From the plot $[m_1]$ vs. $[c_1]$ (see Strömgren's review), we can estimate the spectral type and luminosity class, and thus, the absolute magnitude of the stars in the catalog. We have used Mermilliod's (1987) UBV photometric catalogue, also provided by ADC, to obtain the color excesses and corrected visual magnitudes. The resulting distances are plotted against individual $E(B-V)$ excesses in Fig. 3. In Table 1 we present, for brevity, only the star HD numbers, the excesses, and distances. The individual data can be found in the catalogs mentioned.

Unfortunately, an all-sky survey does not provide enough stars for a good estimate. A second problem is that uvbyβ photometry is not good for the red giant stars which, in general, are the more distant objects. However, from the plot

we infer that the nova cannot be closer than about 1.5 kpc, since the stellar color excesses are significantly smaller, and probably it is farther than about 3 kpc. In addition, a map of the galactic gas by Lucke (1978) shows a large cloud complex at a distance of about 3 kpc. Since the color excess of this cloud seems somewhat large, we can infer that the star might be in or beyond this cloud. So, we will adopt $D \sim 3$ kpc as a plausible, although uncertain, distance for PW Vul.

IV Observational Material

a Optical Spectra

Optical spectrophotometric observations of PW Vul were obtained beginning on September 15, 1985 (day 413) and continued through May 4, 1987 (day 1011). These observations were obtained using the Ohio State University Image Dissector Scanner (Byard et al. 1981) attached to the Perkins 1.8-m Reflector of the Ohio Wesleyan and Ohio State Universities at the Lowell Observatory. These data supplement those already reported by Kenyon and Wade (1986).

Dual 7" diameter entrance apertures and a 600-line-per-mm grating blazed at $\lambda 5500$ were employed which covered about 2600 Å of the spectrum at 10 Å resolution. Two different grating tilts were required to cover the region between 3700 and 8600 Å. Higher dispersion spectra in the Hβ region were obtained on March 27, 1987 using the same telescope and instrument. For these observations, a 1800-line-per-mm grating blazed at $\lambda 4650$ was used, which, when combined with 5" dual entrance apertures, yielded a spectral resolution of about 2.5 Å and covered the region $4400 - 5100$ Å. The spectrum of a quartz–halogen lamp was observed to remove pixel-to-pixel variations in response, and the spectrum of an FeNe–He source provided wavelength calibration. The observations of one or more

7

standard stars permitted the removal of the instrumental response and provided absolute photometric calibration. The reduction procedures are described in Wagner (1986).

In Figure 1a-d, we show a montage of our late-time optical spectra of PW Vul scaled to enhance the weaker features. The principal emission features are identified in Figure 1e from the spectrum obtained on day 413. As shown in Figure 1, the optical spectra consist of a mixture of both permitted and forbidden emission lines of both high and low ionization. The strongest emission lines throughout the late time development are those due to $[O\,III]\,\lambda5007$ and $H\alpha$. Weaker permitted emissions are due to other members of the Balmer series of hydrogen, and also, $He\,I\,\lambda\lambda4471,5876,6678,7065$; $He\,II\,\lambda\lambda4686,5411$; $N\,III\,\lambda4640$, and $N\,V\,\lambda4600$. The strongest forbidden lines arise from $[O\,III]\,\lambda\lambda4959,5007,4363$; $[O\,II]\,\lambda\lambda7320,7330$; $[N\,II]\,\lambda5755$; $[Ne\,III]\,\lambda3869,3968$; $[A\,III]\,\lambda7136$; $[A\,IV]\,\lambda\lambda7237,7263,7170$ (blended with $[A\,III]\,\lambda7136$); and weaker emission due to $[Fe\,II]$. In the later spectra, $[N\,II]\,\lambda\lambda6584,6548$ begin to appear as structure in the $H\alpha$ profile. Many coronal lines are present in the late-time spectra, including those of $[Fe\,VII]\,\lambda6085$, and $[Fe\,VI]\,\lambda5677$. $[Fe\,X]\lambda6374$ is also present as suggested by the anomalous ratio of $[O\,I]\,\lambda6300,6363$.

The absolute strength of the emission lines decreases quickly with time. The relative line strengths also change with time indicating changes in the physical conditions of the ejecta. For example the $[O\,III]\,\lambda5007$ to $H\alpha$ ratio changes from about 1.6 on day 413 to about 3.7 on day 1011 even though the total flux of $[O\,III]$ has decreased by a factor of 16. Note also the changes in the relative strength of the coronal lines, especially $[Fe\,X]\,\lambda6374$. On day 631 the strength of $[O\,I]\,\lambda6300$ is comparable to $[O\,I]\,\lambda6363$ and $[Fe\,X]\,\lambda6374$, but by day 680, $[Fe\,X]$

8

has decreased significantly to the point where the $[O\,I]$ lines have a relative intensity as predicted by the ratio of their transition probabilities. Other obvious changes in relative line strength produced by decreasing density in the emission region include the rapid decrease in intensity of $[N\,II]\lambda5755$ and $[O\,III]\lambda4363$.

In Figure 1f, we show the high dispersion spectrum of PW Vul in the Hβ region obtained on March 27, 1987. Note the well known castellated structure of the emission lines, especially of $[O\,III]\lambda\lambda4959,5007$. At this resolution (150 km/sec), the profiles break up into at least three major components. The expansion velocity as inferred from the line profiles is about 400 km/sec. However, a comparison of the $[O\,III]$ or Hβ line profiles with those of $He\,II\,\lambda4686$ and $N\,III\,\lambda4640$ suggests that the latter two species may arise or originate in a different manner or location than $[O\,III]$.

b   Ultraviolet Spectra

Ultraviolet observations of PW Vul with the IUE satellite began on August 2, 1984, two days after discovery, and continued until June 23, 1988. Unfortunately, many of the early spectra were overexposed as the ultraviolet flux was increasing rapidly. We shall discuss the early spectra elsewhere; here we concentrate on the late time spectra that are suitable for abundance determinations from nebular emission line analyses. In Figure 2a-f we display combined short wavelength prime (SWP) plus long wavelength prime (LWP) spectra obtained during the same shift. In the following paragraphs we shall discuss each of these spectra in turn. Each plot is labeled with the image number from each camera to facilitate archival analysis. Note that while we display the same wavelength scale for most of the spectra, we allow the peak flux to follow the emission lines and it slowly decreases with time.

As shown in Figure 2, the spectrum at late times contained a mixture of both high and low ionization lines with both resonance and intercombination lines present. These spectra are very similar to the optical emission spectra of high redshift quasars. In particular, the presence of $N V \lambda 1240$ indicates a strong ionizing continuum which is borne out by the EXOSAT detection of PW VUL in June 1985 (Ögelman, Krautter, and Beuermann 1987).

Figure 2a shows the spectrum obtained on April 7, 1985, about 9 months after discovery. This is the first spectrum taken after PW Vul had reappeared from behind the sun. The previous spectrum was obtained on November 13, 1984 and still shows a very strong continuum. The spectrum in Fig. 2a is dominated by lines, showing that the expanding shell has become optically thin, the continuum has decreased in intensity, and emission lines characteristic of a low density gas have become prominent. The strongest lines are $N IV] \lambda 1486$, $C IV \lambda 1550$, $N III] \lambda 1750$, $C III] \lambda 1909$, $C II] \lambda 2326$, $Mg II \lambda 2800$, and $O III \lambda 3133$. Other lines are listed in Table 4. The region between about 2000 Å and 2400 Å is underexposed on all spectra and shows the noise level at the short wavelength edge of the LWP camera.

Figure 2b was obtained on June 24, 1985 and while the emission lines are steadily decreasing in intensity, they appear to be retaining virtually the same intensity ratio. However, $Mg II \lambda 2800$ has dropped much faster than $C IV \lambda 1550$. At first glance, the strength of $C II]$, $C III]$, and $C IV$ would suggest that carbon was enhanced in the ejecta. However, they are strong only because of the characteristics of the shell and not, as we show below, because carbon is enhanced in abundance which suggests that one must be careful in interpreting line strengths as indicators of enhanced abundances. Figure 2c was obtained on July

10

16, 1985 and shows the continuing decline of the emission lines. It was followed soon thereafter by the spectrum shown in Figure 2d obtained on July 25, 1985. In this spectrum we extend the red edge to 3400 Å to show that the neon lines are starting to become strong. Below, we show that this is because of the physical conditions in the expanding shell, and not because of any abundance enhancement. The sharp feature just to the red of $O III \lambda 3133$ is a cosmic ray "hit." By October 29, 1985 (Figure 2e), the peak flux in $C IV$ has declined by more than a factor of three and some weaker features are beginning to appear.

The last usable combined spectrum, obtained in March 31, 1986, is shown in Figure 2f. It was somewhat underexposed accounting for the increased noise level. $Mg II$ has clearly disappeared although $C IV$ and $N IV]$ are still present. We believe that all of the "features" between 2000 Å and 2400 Å are noise. A slight rise in the flux is observed towards the red end of the LWP camera; however, we do not know whether this is feature is real.

Our next goal is to derive the chemical composition of the shell, which is an important ingredient for constructing a physical model. To accomplish this, we need to estimate the electronic temperature and density. However, our IUE and optical data were not obtained simultaneously, and in the next section we will attempt to overcome this problem.

V   The Nebular Gas Region

a   Evolution of Emission Lines

The spectra show emission lines typical of the nebular phase of a nova. The intensities for a recombination line like $H\beta$ are collected in Table 2, which also includes its absorption-corrected intensity and its luminosity, assuming the

11

distance of 3 kpc just derived. In Table 3, we present the ratios with respect to $H\beta$ for several optical lines. Each entry has two lines: the observed ratio, and the reddening-corrected ratio for $E(B-V) = 0.60$. The ultraviolet emission lines are listed in Table 4, which has three entries per line: the observed flux, the observed ratio, and the corrected ratio. All reddening corrections have been calculated using the fits to the interstellar extinction curve obtained by Seaton (1979). We will use these data to derive temperatures and densities and to compare them to model calculations. Figs. 5 and 6 show the behavior of the [OIII] lines ratios as a function of time.

Fig. 4 shows that $H\beta$ declines monotonically from day 235 to day 1011, as can be expected for a matter-bounded photoionized expanding shell (cf. section III.a). A least squares fit of the data allows us to express the flux in $H\beta$ as a power law given by

$$f(H\beta) = const \cdot t^{-3.84} \quad . \tag{1}$$

If Hydrogen is assumed to be fully ionized, then the intensity of $H\beta$ is given by

$$I(H\beta) \simeq h\nu_{H\beta} N_e N_p \, \alpha_{H\beta}^{eff} \cdot V \quad , \tag{2}$$

where $\alpha_{H\beta}^{eff}$ is the effective recombination coefficient for $H\beta$ and V is the volume of the emitting region. If we consider the mass of the ejecta $M = \mu N_e \cdot V$ to be constant, then the intensity of $H\beta$ has a linear dependence on N_e, and both have the same time dependence. The deduced slope of -3.84, is a somewhat faster decline than that corresponding to a free expansion of the shell, t^{-3}.

b Temperatures and Densities

We use two procedures to calculate densities and temperatures for the nebular phase. In the first case, we use $[OIII]\,\lambda\lambda 4959, 5007$, $[OIII]\,\lambda 4363$, and $H\beta$. In the second case, we use both optical [OIII] lines and the ultraviolet doublet $[OIII]\,\lambda\lambda 1660, 1666$. This will give us a check on the derived values. This check is necessary since we do not have simultaneous observations in the optical and ultraviolet, and the scarcity of the data may introduce large errors during the interpolation. The techniques used to calculate line intensities as function of the level populations, the density, and the temperature of the gas are described by Osterbrock (1988).

Fig. 5 shows the observed $[OIII]/H\beta$ intensity ratio as a function of time. The figure suggests that at about day 450-500, the ^1D level emitting the $\lambda\lambda 4959, 5007$ line reach its critical density, where collisional excitation and radiative deexcitation are equal. Thus, we can expect that by $t_2 = 680$ days, the density of O^{++} was well below its critical value of $N_{crit} \sim 7 \times 10^5\,cm^{-3}$, so collisional de-excitation is negligible. On the other hand, at $t_1 = 235$ days, we can assume that the levels are thermalized, since $N \gg N_{crit}$ and LTE can be assumed for the level populations.

A detailed balance equation lets us write the ratio of the densities in the $^1D_2$ and $^3P_{1,2}$ levels giving rise to $\lambda\lambda 4959, 5007$. Then, we can easily obtain the intensity ratios for this blend with respect to $H\beta$ in the high (at day t_1), and in the low (at day t_2), density limits. If we assume that the electron temperature is constant throughout the interval (which is not be a bad assumption considering the observational uncertainties), we can take the ratio between both expressions to obtain a relation between density and temperature at time t_1. This is given by

13

$$N_e(t_1)/\sqrt{T_e(t_1)} = 7128.7 \times j_{4959,5007}(t_2)/j_{4959,5007}(t_1) . \qquad (3)$$

A second relation between $N_e(t_1)$ and $T_e(t_1)$, can be obtained by calculating the populations of the $^1S_0$ and $^1D_2$ levels of O^{++}, which form the line at $\lambda 4363$, and then forming the intensity ratio j(4363)/j(4959,5007). We have used the solution to the five-level atom, using the atomic parameters from Mendoza (1982). The complete solution is quite involved, but it is only function of the electron density and temperature,

$$j_{4363}/j_{4959,5007} = f[N_e(t_1), T_e(t_1)] . \qquad (4)$$

Both equations should allow us to determine the temperature and the density, at time t_1, and the density at any other time can be obtained from the constraint imposed by $H\beta$, namely,

$$N_e(t_2)/N_e(t_1) = (t_2/t_1)^{-3.84} . \qquad (5)$$

The results are summarized in Table 5, for both values of color excesses. The critical density of [OIII]$\lambda\lambda 4959, 5007$ occurs at about day 470, as suggested by inspection of Fig. 5.

Another way to estimate densities and temperatures is by using the set of [OIII] lines at $\lambda\lambda 1660, 1666, \lambda 4363$ and $\lambda\lambda 4959, 5007$. The first two lines originate in the $^5S_2^0 - {}^3P_{1,2}$ levels of O^{++}. When we form the ratios j(1660,1666)/ j(4959,5007) and j(4363)/j(4959,5007), we obtain expressions dependent on the electron density and temperature, and both parameters can in principle be found. In this case, however, we do not have simultaneous UV and optical observations, and an approximate solution can be only obtained by interpolating in the data.

Another important source of error, especially for the UV lines, are the uncertainties in $E(B-V)$. To see this, we plotted curves of equal intensity ratio in the plane $\log N_e - \log T_e$ (Figure 7). The curves correspond to the minimum and maximum values of j(1660,6)/j(4959,5007) obtained by applying color excesses with the estimated errors. We include a simple curve for j(4363)/j(5007) since this ratio changes very little with reddening. From the plot, we estimate that the uncertainty in the electron density is about $0.5 \times 10^6 cm^{-3}$ and, in the temperature, about 2,000 K, due to reddening. The results obtained from this method are also included in Table 6.

In summary, our results suggest that $T_e \sim 13,000K$ and the density falls from about $4 \times 10^6 cm^{-3}$, 11 months after the explosion, to about $10,000 - 100,000\ cm^{-3}$, one year later. Based on these results we can derive the abundances in the ejecta.

c Chemical Composition

For the most part, the methods and atomic parameters needed to derive the abundances have been taken from Osterbrock (1988). Electron densities and temperatures are also used as calculated in the previous section. The errors in the abundances are estimated assuming that the uncertainty in the temperature is ~ 2000 K.

Helium   The abundances of single and double ionized helium can be obtained from the intensities of He I $\lambda 5876$ and He II $\lambda 4686$ relative to Hβ, respectively. Assuming pure radiative recombination, the density of helium with respect to hydrogen can be easily obtained by assuming that $He/H = He^+/H^+ + He^{++}/H^+$, and the ion abundances are given by

$$\frac{j(HeI)}{j(H\beta)} = \frac{N(He^+)}{N(H^+)} \frac{\alpha_{HeI}(T)}{\alpha_{H\beta}(T)} \frac{4861}{5876} \tag{6}$$

$$\frac{j(HeII)}{j(H\beta)} = \frac{N(He^{++})}{N(H^+)} \frac{\alpha_{HeII}(T)}{\alpha_{H\beta}(T)} \frac{4861}{4686} \tag{7}$$

where $\alpha_\lambda(T)$ is the recombination coefficient for the specified line. The ratio of recombination coefficients is not very sensitive to temperature (Peimbert, 1975).

However, the assumption stated above would make us overestimate the abundance of helium. Collisional excitation from the metastable $2s\,^3S$ level of He I can be important and it will contribute to the observed intensity of recombination lines like $\lambda 5876$. Clegg (1987) provides simple formulae to account for this effect. The correct abundance of He^+/H^+ is obtained by multiplying the abundance derived from equation (6) by the factor $(1 + C/R)^{-1}$, where C/R is the ratio of excitations by collissions to recombinations. The abundances of ionized helium, both uncorrected and corrected by collissions, and the total abundances are listed in Table 6.

A simple average of these data gives $He/H = 0.092 \pm 0.009$, which is almost coincident with cosmic abundances.

Oxygen The line ratio $j(4959, 5007)/j(H\beta)$ can be used to obtain O^{++}/H^+. Since He and O both have about the same ionization potentials, we assume that $O^{++}/He^+ \simeq O/He$, and, by using the He abundances just obtained, we obtain the O/H abundance ratios listed in Table 7. An average of these results gives $O/H = (1.29 \pm 0.75) \times 10^{-3}$. The probable error is mainly influenced by the uncertainties in the temperature.

Nitrogen The nitrogen abundance can be expressed in terms of the ionic abundances as

$$N/H = (N^+/H^+) \cdot (O/O^+) \qquad (8)$$

$$O/H^+ = (O^+ + O^{++})/H^+. \qquad (9)$$

and the ionic abundances are obtained, as before, from the emissivity ratios $j([NII]\,5755)/j(H\beta)$, for N^+/H^+, $j([OIII]\,5007)/j(H\beta)$, for O^{++}/H^+, and $j([OII]\,7330)/j(H\beta)$, for O^+/H^+. Note that in doing this, we are assuming that O^+ has the same temperature as O^{++}. The observational errors here might be somewhat larger since $[OI]\,\lambda 7330$ is a relatively weak line. Again, refer to Table 7. The average is $N/H = (5.1 \pm 4.2) \times 10^{-3}$, which is over 50 times the solar abundance.

Neon The most useful line is [NeIII] $\lambda 3869$, and $Ne/O \sim Ne^{++}/O^{++}$ can be assumed, again using the [OIII] 5007 line. Results are collected in the final column of Table 7. In forming the average, we gave half weight to the uncertain observation at day 631. The result is $Ne/O \sim 0.037$, or $Ne/H = (4.5 \pm 2.6) \times 10^{-5}$, i.e., about half the solar abundance.

Carbon The ratio of ultraviolet lines $j([CIII]\,1907,1909)/j([OIII]\,1660,1666)$ give the ion abundance $C^{++}/O^{++} \sim C/O$. Table 4 shows the line ratios. For a temperature of 13,200 K, $C/O = 0.45$ at day 330, and $C/O = 0.17$ at day 681. Using the previously derived oxygen abundance, we find an almost solar abundance of $C/H = (4.0 \pm 2.3) \times 10^{-4}$.

Summary of Abundances In Table 8 we collect all average abundances and compare them to accepted solar values. It can be seen that the ejecta has approximately solar composition, with the exception of nitrogen, which is enhanced even including the observational errors. A higher nitrogen abundance is to be expected if the star was burning hydrogen through a non-equilibrium CNO cycle (see, for instance, Starrfield, Sparks, and Truran 1986).

VI The Coronal Line Region

The optical and IUE spectra suggest that the continuum spectrum is predominantly free-free emission. The absence of a strong Balmer jump and the strength of the continuum relative to Hβ are clear indications that the gas producing the continuum is very hot. We computed the observed continuum fluxes in the form f_ν ($erg\ cm^{-2}\ sec^{-1}\ Hz^{-1}$), from the equivalent widths and intensities of several ultraviolet lines (see Table 9), for day 330. Also, we added infrared fluxes for day 319 published by Gehrz *et al.* (1988). Fig. 8 shows the observed continuum intensities relative to the intensity of Hβ (in units of Hz^{-1}), for day 330.

To account for the observed continuum, we first try a fit with the theoretical predictions from nebular theory. To do this, we assume that the observed continuum flux f_ν ($erg\,sec^{-1}cm^{-3}Hz^{-1}$) can be expressed as the sum of the continuum fluxes of the cooler "nebular" gas and the hotter "coronal" gas. Both fluxes, relative to the intensity of Hβ, can be expressed in terms of their respective continuous emission coefficients, electron densities and volumes of the emitting region. Assuming that Hβ is formed in the nebular region, they are given by,

$$\frac{f_{\nu,cor}}{I_{H\beta}} = \frac{(N_e N_+)_{cor} V_{cor} \gamma_{\nu,cor}}{(N_e N_+)_{neb} V_{neb} 4\pi j_{H\beta}} \qquad (10)$$

$$\frac{f_{\nu,neb}}{I_{H\beta}} = \frac{\gamma_{\nu,neb}}{4\pi j_{H\beta}} \qquad (11)$$

Ferland (1980) calculated the continuous emission coefficients of H and He as a function of electron temperature. The lower curve of Fig. 8 shows the resulting nebular phase continuous emission relative to the $H\beta$ emission coefficient, from a mixture of H and 10% He (as calculated in Section V.c), at $T_e = 10^4 K$. This theoretical continuum includes both free-free and bound-free transitions. For the optical continuum we used the continuous coefficients tabulated by Osterbrock (1988), since they include more accurate Gaunt factors. We can see from the figure, that the continuum emission from the "nebular" phase is too weak to explain the observed free-free spectrum, and it also predicts a strong Balmer jump, which is not observed. This suggests that the nebular gas represents some fraction of the total mass, and the rest is at a substantially higher temperature. The hot gas radiation is mainly a free-free continuum and X-ray lines, with very little recombination or collisionally excited line emission in the optical.

We now estimate the contribution to the continuum from very hot gas. We adopted a combination of H and He continua at $T = 10^6 K$, as tabulated by Ferland (1980). Dividing the observed relative density flux by Eq. 11, we obtain,

$$\frac{f_{\nu,obs}/I(H\beta)}{\gamma_{\nu,neb}/4\pi j_{H\beta}} = 1 + \frac{E_{cor}\gamma_{\nu,cor}}{E_{neb}\gamma_{\nu,neb}} , \qquad (12)$$

where the emission measure $E \sim N_e^2 V$. The left-hand side of this equation can be obtained from Fig. 8, where we choose to fit the optical region ($\lambda 5550$). On the right side, we obtain the ratio of continuous coefficients, γ, from Ferland's (1980) tabulations, and, then, we can solve for the ratio of emission measures. This gives the amount of hot gas to add to the nebular gas to fit the observed spectrum, as the equation above indicates. We obtained a factor of about 5.5, and the resulting

spectrum is shown as a solid line in Fig. 8. The fit, specially the Balmer jump, is greatly improved, except for an infrared excess, which can be atributed to thermal emission from dust in the shell (Gehrz *et al.* 1988), which, as mentioned in section II, started to develop by day 280. In Fig. 8, we fit the infrared continuum with a blackbody at 590 K. Since this excess is still small, the temperature is only a crude estimate.

We can now use the ratio of emission measures to estimate the mass of coronal gas. Recalling that the mass is given by $M = \mu_e N_e V$, we obtain,

$$\frac{N_{cor}^2 V_{cor}}{N_{neb}^2 V_{neb}} = \frac{N_{cor} M_{cor}}{N_{neb} M_{neb}} = 5.50 .$$

If the nebular and coronal line regions are in pressure equilibrium, then, the ratio of electron densities equals the inverse ratio of the temperatures, and therefore, $M_{cor} \sim 550 \times M_{neb}$. If, rather, they have the same density, then $M_{cor} \sim 5.5 \times M_{neb}$. In either case, we see that a surprisingly large mass is in the coronal line region. The mass of nebular phase gas can also be calculated from the luminosity emitted in Hβ and the nebular electron density, which we obtained in the previous section. Then, at day 330, $L_{H\beta} \sim 2.71 \times 10^{34} \; erg \; sec^{-1}$, and $N_{neb} = (3.4 \pm 0.5) \times 10^6 \; cm^{-3}$, the nebular mass is

$$M_{neb} \sim \frac{m_p L_{H\beta}}{N_{neb} \gamma_{H\beta}} = (1.1 \pm 0.3) \times 10^{29} \; g; \tag{13}$$

that is, the mass of nebular gas is $\sim 5.3 \times 10^{-5} M_\odot$, and, therefore, the total mass of the ejecta lies in the range $3 \times 10^{-4} - 3 \times 10^{-2} M_\odot$.

Finally, we can use these estimates to evaluate the energetics of the ejecta. Assuming an expansion velocity of 600 km/sec, the kinetic energy is of the order of 1.1×10^{45} to 1.1×10^{47} ergs, by day 330.

VII   A Model of the Ejecta

a   Model Parameters

We used a photoionization model of the ejecta to reproduce the observed spectrum as a check on our abundances. We chose to match the optical data for day 413, for which we felt the abundances and observations were best estimated, and made a rough interpolation for some of the available ultraviolet lines. The model was calculated using the photoionization code CLOUDY (Version 72: Ferland 1989).

The model consists of an expanding spherical shell, which has a hydrogen density of $6.3 \times 10^5 \, cm^{-3}$, at day 413. Based on an expansion velocity of 600 km/sec, as discussed above, we adopted a radius of $2 \times 10^{15} \, cm$ for day 413. For the continuum, we chose a luminosity of $6.3 \times 10^{36} \, erg/sec$ and shape given by optically thin hydrogen bremssthralung at a temperature of $2 \times 10^6 K$. These numbers were chosen to give an aceptable match of the observed helium ionization and the luminosity of Hβ. This luminosity is also consistent with the observed brightness of the optical free-free continuum.

The metal abundances had to be increased by about 20% from those given in Table 8 to have a reasonable match of the ultraviolet spectrum. The only exception was carbon, which had to be adjusted by a substantially larger factor. We should remember that our derivation of carbon abundance is based on only two days and, therefore, highly uncertain. The set of abundances we used is as follows, as a fraction of solar abundances: He, 0.9; C, 2.4; N, 60; O, 1.8; all other elements, 1.2 times solar.

b Comparison with the Observations

In Table 10, we present a comparison between the predictions of this model and
the observed intensities. It can be seen that, in most cases, they agree within a
factor of 2 or less, which we find reasonable whithin the uncertainties discussed in
previous sections.

Silicon depletion? We can use these results to further investigate the problem of
dust production already mentioned. If dust has been formed in the ejecta, we
expect the observed intensities of the silicon lines to be lower than those predicted
for our model, since these atoms are incorporated in the dust grains. On the other
hand, the intensity of a line such as $Mg\,II\,\lambda2798$ will not show signs of depletion,
since this element does not play a significant role in forming dust.

Our data fail to show $Si\,III]\,\lambda1892$ at all dates considered here. For dates
close to our model calculation, the detection limit of this line, is of the order of
$2 \times 10^{-14} erg\,cm^{-2}sec^{-1}$ (2σ), which implies that the intensity of $Si\,III]\,\lambda1892$
relative to Hβ is ≤ 0.12, corrected for reddening. Our model (see Table 10),
predicts a relative intensity of 0.24, for a nearly solar abundance. The observed
relative intensity of $Mg\,II\,\lambda2798$, interpolated for day 413, is about 0.6, while our
model predicts a ratio of 0.4. Both figures are comparable within the
observational errors. From these results, we infer that silicon might be depleted by
at least a factor of 2. This depletion factor might be consistent with the small
production rate reported by Gerhz *et al.* (1988).

High Excitation Lines In previous work on other novae (e.g., Nova Cygni 1975;
Ferland, Lambert, and Woodman 1977), it has been shown that the presence of
high excitation lines is a clear indication of the existence of a hot coronal line

22

region. A useful line for this purpose is $[Fe\,X]\,\lambda6374$, which is blended with $[O\,I]\,\lambda6363$, but it is possible to separate both contributions by comparing the intensity of this blend with the neighboring line $[O\,I]\,\lambda6300$. The ratio of transition probabilities for both $[O\,I]$ lines is $A(6363)/A(6300) = 0.32$ (Osterbrock, 1988). At days 73, 309, and 413, the reddening corrected ratios were 1.20, 0.54, and 0.57, which implies that $[Fe\,X]\,\lambda6374/[O\,I]\lambda6300 \sim 0.88$, 0.22, and 0.24, respectively.

As indicated in Table 10, the model predicts that, at day 413, this ratio should be about 0.1 in the warm component of the ejecta. This is somewhat lower than the observed value. We conclude that these ions have become too weak in the coronal line region at this point of the outburst, and the observations reflect their presence in both the nebular and the coronal gas.

VIII   Discussion and Summary

In this final section, we summarize the topics presented in this paper and discuss some of their implications.

The distance to the nova is of the order of 3 kpc, which is within the range of previously determined measures.

Ultraviolet lines of [OIII] can be used in conjunction with the optical lines to obtain electron temperatures and densities. The results are uncertain due to errors in the reddening and in the numerical interpolation of the data, if the optical and ultraviolet observations are not simultaneous.

We obtained a fairly reliable set of abundances for the ejecta of PW Vul. The only element with a significantly higher-than-solar abundance is nitrogen. Some researchers have reported anomalous abundances for some specific elements in other novae (e.g., neon; Gehrz, Grasdalen, and Hackwell, 1985), a phenomenon

that has been interpreted as a consequence of the evolutionary state of the progenitor star at the time of the outburst (Starrfield, Sparks, and Truran, 1986). In this case, the high nitrogen abundance could be a by-product of hydrogen burning through the CNO cycle. The nearly solar abundances of C, O, and Ne indicates that this star did not go as far in the burning cycle at the time of the outburst. This is consistent with a very slow nova.

The ejecta has a hot ($T \sim 10^6 K$) component where lines of highly ionized species and the free-free continuum originate, and a warm ($T \sim 10^4 K$) component which give rise to the recombination lines. Free-free emission from the hot component is the main contribution to the optical and ultraviolet continuum, and may be the source of heating of the ejecta during the early decline.

A third component to the observed continuum is characterized by thermal emission, presumably from dust. Silicon might be depleted for at least a factor of two over solar abundances, providing further evidence for the presence of this material.

IX   Acknowlegments

Aeronautics and Space Administration through grant NAG 5-481.

Table 1: Photometry and distances in the field of PW Vul

HD #	$E(B-V)$	$D(pc)$
180 502	0.06	47.9
180 553	0.15	316.2
180 583V	0.07	1202.
180 584	0.36:	2399.
180 615	0.08	57.5
180 917	0.11	91.2
181 602	0.08	69.2
182 008	0.09	83.2
182 255	0.01	158.5
182 568	0.14	263.0
182 618	0.07	302.0
182 807	0.03	1000.
183 032D	0.11	57.5
183 033	0.23	10470.
183 560	0.12	100.0
183 614	0.05	631.0
183 914	0.00	114.8
184 058	0.05	120.2
184 151	0.12	60.3
184 384	0.14	83.2
184 720	0.36	8710.
184 979	0.06	63.1
184 998	0.00	138.0
185 242	0.15	229.1
185 269	0.08	33.1
185 270	0.04	87.1

Table 2: Light Curve of $H\beta$

t	$I(H\beta)$	$I(H\beta)_0$	$L(H\beta)$
235	1.68(-11)	9.23(-11)	9.94(34)
309	5.90(-12)	3.24(-11)	3.49(34)
413	2.60(-12)	1.43(-11)	1.54(34)
631	2.84(-13)	1.57(-12)	1.69(33)
680	2.62(-13)	1.44(-12)	1.55(33)
1011	7.71(-14)	4.2 (-13)	4.52(32)

Table 3: Optical Emission Lines[a]

Element	Days since outburst					
	235	309	413	631	680	1011
$H\beta$	1.00	1.00	1.00	1.00	1.00	1.00
$HeI5876$	0.15	0.15	0.14	0.20	0.15	0.12
	0.10	0.10	0.10	0.14	0.10	0.08
$HeII4686$	0.29	0.36	0.40	0.47	0.49	0.57
	0.31	0.39	0.43	0.51	0.53	0.62
$[NII]5755$	0.82	1.46	1.98	2.16	1.55	0.68
	0.60	1.06	1.44	1.57	1.13	0.49
$[OI]6300$	—	0.15	0.30	0.43	0.45	0.30
	—	0.09	0.19	0.27	0.28	0.19
$[OII]7330$	—	0.66	3.23	1.15	0.76	0.35
	—	0.33	1.62	0.58	0.38	0.18
$[OIII]4363$	1.08	1.80	1.53	0.99	0.88	0.46
	1.36	2.28	1.93	1.25	1.11	0.58
$[OIII]4959+5007$	3.80	9.71	23.19	43.31	45.42	49.94
	3.59	9.18	21.93	40.96	42.95	47.23
$[NeIII]3869$	0.27	0.51	0.75	0.38:	0.56	—
	0.42	0.79	1.16	0.59:	0.86	—
$[FeVII]6087$	—	0.19	0.29	0.44	0.27	0.36
	—	0.13	0.19	0.29	0.18	0.24

[a]Each entry, line 1: observed ratio; 2: corrected ratio

28

Table 4: Ultraviolet Emission Lines[a]

Element	Days since outburst			
	253	331	340	681
$HeII$1640	3.30(-12)	1.08(-12)	1.22(-12)	—
	0.26	0.25	0.30	—
	2.58	2.48	2.98	—
CIV1549	—	1.30(-11)	1.12(-11)	5.42(-13)
	—	2.82	2.62	2.06
	—	31.38	28.59	22.48
NV1240	—	5.13(-12)	4.75(-12)	3.40(-12):
	—	1.10	1.11	1.29
	—	30.31	30.58	35.54
NIV]1486	—	7.08(-12)	7.29(-12)	5.56(-13)
	—	1.51	1.71	2.11
	—	18.11	20.50	25.30
$NIII$]1750	—	6.23(-12)	4.89(-12)	1.47(-13)
	—	1.33	1.15	0.56
	—	12.74	11.01	5.36
OIV]1402	3.36(-12)	1.15(-12)	9.93(-13)	—
	0.22	0.25	0.23	—
	3.08	3.50	3.22	—
[$OIII$]1660,6	4.31(-12)	8.43(-13)	1.10(-12)	1.32(-13)
	0.29	0.18	0.26	0.50
	2.80	1.76	2.52	4.89
$MgII$2798	—	2.00(-12)	5.24(-13)[b]	7.76(-14):
	—	0.44	0.15	0.30:
	—	1.63	0.56	1.11:

[a]Line 1: flux in $erg\,cm^{-2}sec^{-1}$; 2: ratio wrt $H\beta$; 3: corrected ratio

[b]Observation made on day 353

29

Table 5: Electron Temperatures and Densities

day	$N_e(cm^{-3})$	T_e(K)	$N_e(cm^{-3})$	T_e(K)
	$E(B-V) = 0.45$		$E(B-V) = 0.60$	
a) lines 4363, 4861, 4959/5007				
253	7.7(6)	13,200	7.6(6)	13,200
331	2.8(6)	"	2.7(6)	"
340	2.5(6)	"	2.4(6)	"
681	1.7(5)	"	1.7(5)	"
b) lines 1660/1666, 4363, 4959/5007				
253	1.6(6)	23.300	3.0(6)	21,900
331	3.3(6)	11,900	4.0(6)	12,700
340	2.7(6)	12,400	2.2(6)	15,800
681	3.2(4)	16,000	1.0(4):	18,300

Table 6: Abundance of Helium

day	He^+/H^+		He^{++}/H^+	He/H
	no coll.	coll.		
235	.074	.050	.027	.077
309	.074	.050	.033	.083
413	.074	.050	.037	.087
631	.104	.071	.043	.114
680	.074	.051	.045	.096
1011	.059	.041	.052	.093

Table 7: Abundances of Oxygen, Nitrogen and Neon

day	O^{++}/H^+	O/H	N^+/H^+	O^+/H^+	N/H	Ne/O
235	6.68(-4)	1.03(-3)	—	—	—	0.038
309	6.89(-4)	1.14(-3)	4.38(-5)	0.62(-5)	4.94(-3)	0.044
413	7.55(-4)	1.31(-3)	5.56(-5)	2.70(-5)	1.61(-3)	0.046
631	7.55(-4)	1.21(-3)	5.93(-5)	1.02(-5)	4.43(-3)	0.020:
680	7.49(-4)	1.41(-3)	4.25(-5)	0.65(-5)	4.93(-3)	0.030
1011	7.21)(-4)	1.63(-3)	3.77(-5)	0.28(-5)	9.68(-3)	—

Table 8: Abundances in PW Vul

Element	PW Vul	Sun	PW/Sun
He/H	0.09	0.10	0.9
C/H	4.0(-4)	4.7(-4)	0.8
N/H	5.1(-3)	9.8(-5)	52.0
O/H	1.3(-3)	8.3(-4)	1.6
Ne/H	4.8(-5)	1.0(-4)	0.5

Table 9: Continuum Fluxes at day 330[a]

λ	f_ν
1240	8.533(-15)
1639	9.175(-15)
1663	4.894(-15)
1749	1.963(-14)
1909	1.394(-14)
2798	1.944(-14)
3133	1.571(-14)
5550	1.418(-14)
2.3	1.592(-14)
3.6	2.557(-14)
8.7	1.011(-13)
10.0	8.733(-14)
11.4	7.871(-14)

[a]Last 5 entries in microns

Table 10: A Model for Day 413[a]

Line	Observed	Model
$H\beta$	34.2	34.2
$H\alpha$	—	2.78
$[N\,II]\,6584$	—	8.69
$H\alpha + [N\,II]$	9.62	11.47
$He\,I\,1640$	3.:	2.2
$He\,I\,5876$	0.10	0.09
$He\,II\,4686$	0.42	0.41
$C\,III]\,1909$	7:	9.5
$C\,IV\,1549$	27.5:	17.4
$[N\,II]\,5755$	1.4	0.9
$N\,III]\,1750$	10.:	13.9
$N\,IV]\,1486$	21.5:	14.6
$N\,V\,1240$	32.:	32.3
$[O\,I]\,6300$	0.2	0.4
$[O\,II]\,7325$	1.6	0.2
$[O\,III]\,1660 + 1666$	3.:	1.2
$[O\,III]\,4363$	1.8	1.1
$[O\,III]\,4959 + 5007$	22.0	22.0
$O\,IV]\,1402$	3. :	0.8
$[Ne\,III]\,3869$	1.1	1.2
$Mg\,II\,2798$	0.6	0.4
$[Fe\,VII]\,6087$	0.2	0.1
$[Fe\,X]\,6374$	0.24	0.1
$< Te\,[O\,III] > K$	13,200	12,700
$< Ne > cm^{-3}$	1.14(6)	7.1(5)

[a] Entries give line intensities with respect to $H(\beta)$.
The first entry is $\log L(H\beta)$ in erg/sec.

References

Byard, P. L., Foltz, C. B., Jenkner, H., and Peterson, B. M. 1981. *P. A. S. P.*, **93**, 147.

Clegg, R. E. S. 1987. *M.N.R.A.S.*, **229**,31p.

Duerbeck, H. W., Geffert, M., Nellse, B., Dummler, R., and Nolte, M. 1984. *Inf. Bull. Var. Stars No.* 2641.

Ferland, G. J. 1978. *Ap. J.*, **219**, 589.

Ferland, G. J. 1980. *P. A. S. P.*, **92**, 596.

Ferland, G. J. 1989. *Astronomy Dept. Internal Report* 89-001 (The Ohio State University).

Ferland, G. J., and Shields, G. A. 1978. *Ap. J.*, **226**, 172.

Ferland, G. J., Lambert, D. L., and Woodman, J. H. 1977. *Ap. J.*, **213**, 132.

—. 1986. *Ap. J. Suppl.*, **60**, 375.

Gehrz, R. D., Grasdalen, G. L., and Hackwell, J. A. 1985. *Ap. J. (Letters)*, **298**, L47.

Gehrz, R. D., Harrison, T. E., Ney, E. P., Matthews, K., Neugebauer, G., Elias, J., Grasdalen, G. L., and Hackwell, J. A. 1988. *Ap. J.*, **329**,894.

Grasdalen, G., and Joyce, R. R. 1980. Preprint.

Hacke, G. 1987. *Inf. Bull. Var. Stars No.* 2979.

Hauck, B., and Mermilliod, M. 1985. *Astr. Ap. Suppl.*, **60**, 61.

Kenyon, S. J., and Wade, R. A. 1986. *P. A. S. P.*, **98**, 935.

Lucke, P. B. 1978. *Astr. Ap.*, **64**,367.

Mendoza, C. 1982. In *IAU Coll. 103 Planetary Nebulae*, ed. D. R. Flower (Dordrecht: D. Reidel), p. 143.

Mermilliod, J. C. 1987. *Astr. Ap. Suppl.*, **71**, 119.

Neckel, Th., and Klare, G. 1980. *Astr. Ap. Suppl.*, **42**, 251.

Ögelman, H., Krautter, J., and Beuermann, K. 1987. *Astr. Ap.*, **177**,110.

Osterbrock, D.E. 1989. *Astrophysics of Gaseous Nebulae and Active Galactic*

Nuclei (Mill·Valley, CA: University Science Books).

Peimbert, M. 1975. *Ann. Rev. Astron. Ap.*, **13**, 113.

Schild, R.E. 1976. *Ap. J. (Letters)*, **209**, L35.

Seaton, M. J. 1978. *M.N.R.A.S.*, **185**, 5p.

Seaton, M. J. 1979. *M.N.R.A.S.*, **187**, 73p.

Shara, M. M. 1989. *P. A. S. P.*, **101**,5.

Sowell, J. R., Laird, J. B., and Thorstensen, J. R. 1985. *Inf. Bull. Var. Stars No.* 2700.

Starrfield, S. 1988. In *Multiwavelength Astrophysics*, ed. F. A. Córdova (Cambridge University Press), p. 159.

Starrfield, S., Sparks, W. M., and Truran, J. W. 1986. *Ap. J. (Letters)*, **303**, L5.

Stromgren, B. 1966. *Ann. Rev. Astron. Ap.*, **4**, 433.

Wagner, R. M. 1986. *Ap. J.*, **308**, 152.

AUTHORS' ADRESSES:

GARY J. FERLAND and PEDRO SAIZAR: Department of Astronomy, The Ohio State University, Columbus, OH 43210

SCOTT J. KENYON: Center for Astrophysics, 60 Garden Street, Cambridge, MA 02138

WARREN M. SPARKS, Los Alamos National Laboratory, MSF 663 X-3, Los Alamos, NM 87545

SUMNER STARRFIELD and L. L. STRYKER, Department of Physics and Astronomy, Arizona State University, Tempe, AZ 85287

JAMES W. TRURAN: Department of Astronomy, University of Illinois, Urbana, IL 61801

R. MARK WAGNER: Lowell Observatory, 1400 W Mars Hill Road, Flagstaff, AZ 86001

ROBERT E. WILLIAMS: Cerro Tololo Inter-American Observatory, Casilla 603, La Serena, Chile

FIGURE CAPTIONS

Fig. 1: Montage of optical spectra of PW Vul during outburst. *(a)* September 25, 1985 (day 413), *(b)* April 20, 1986 (631), *(c)* June 8, 1986 (680), *(d)* May 4, 1987 (1011). *(e)* Enlargement of the spectrum of PW Vul obtained on September 15, 1985 showing the principal emission features. Note the presence of both permitted and forbidden lines of both high and low ionization. *(f)* High dispersion spectrum obtained on March 27, 1987 in the Hβ region. Note the castellated structure of the emission lines implying an expansion velocity of about 400 km/sec. (Inset) Enlargement of the region between 4400 and 4900 Å showing the line profiles of $N\,III\,\lambda4640$, $He\,II\,4686$, and Hβ.

Fig. 2: Ultraviolet spectra of PW Vul during outburst. *(a)* April 7, 1985 (day 253), *(b)* June 24, 1985 (331), *(c)* July 16, 1985 (353), *(d)* July 25, 1985 (362), *(e)* October 29, 1985 (458), *(f)* March 31, 1986 (611).

Fig. 3: Reddening in the field of PW Vul. The dashed line is based on Neckel and Klare's (1980) work. The full line is just a linear growth of absorption with distance typical for our Galaxy. The "stars" represent field stars. "Sun" symbols are the available estimates for PW Vul, from left to right: Duerbeck et al. (1984), this paper, Gehrz et al. (1988).

Fig. 4: Light curve of Hβ including a least square fit of the data.

Fig. 5: Evolution of [OIII] lines. The upper curve corresponds to the intensity ratio $R = I([OIII]\,4959, 5007)/I(H\beta)$; the lower curve to $R = I([OIII]\,4363)/I(H\beta)$.

Fig. 6: Light curve of $R = I([OIII]\,4959, 5007)/I([OIII]\,4363)$.

Fig. 7: Electron temperature vs. density from [OIII] lines. Full lines correspond to $\lambda4363/\lambda\lambda4959,5007$ and an E(B-V)=0.60. Dashed lines correspond to $\lambda\lambda1660,1666/\lambda\lambda4959,5007$ and E(B-V)=0.54. Dot-dashed lines are for the same ratio, but E(B-V)=0.66. The intersection of the full line with the other two gives the errors in the measurement of density and temperature.

Fig. 8: The continuum spectrum of PW Vul relative to $H\beta$. Dots represent observed continuum intensities. The dotted line includes free-free and bound-free emission by H and He at 10,000 K (nebular component). The upper curve includes hot coronal gas (10^6 K) as described in the text. A blackbody continuum at 690 K was also added to fit the infrared excess to the left.
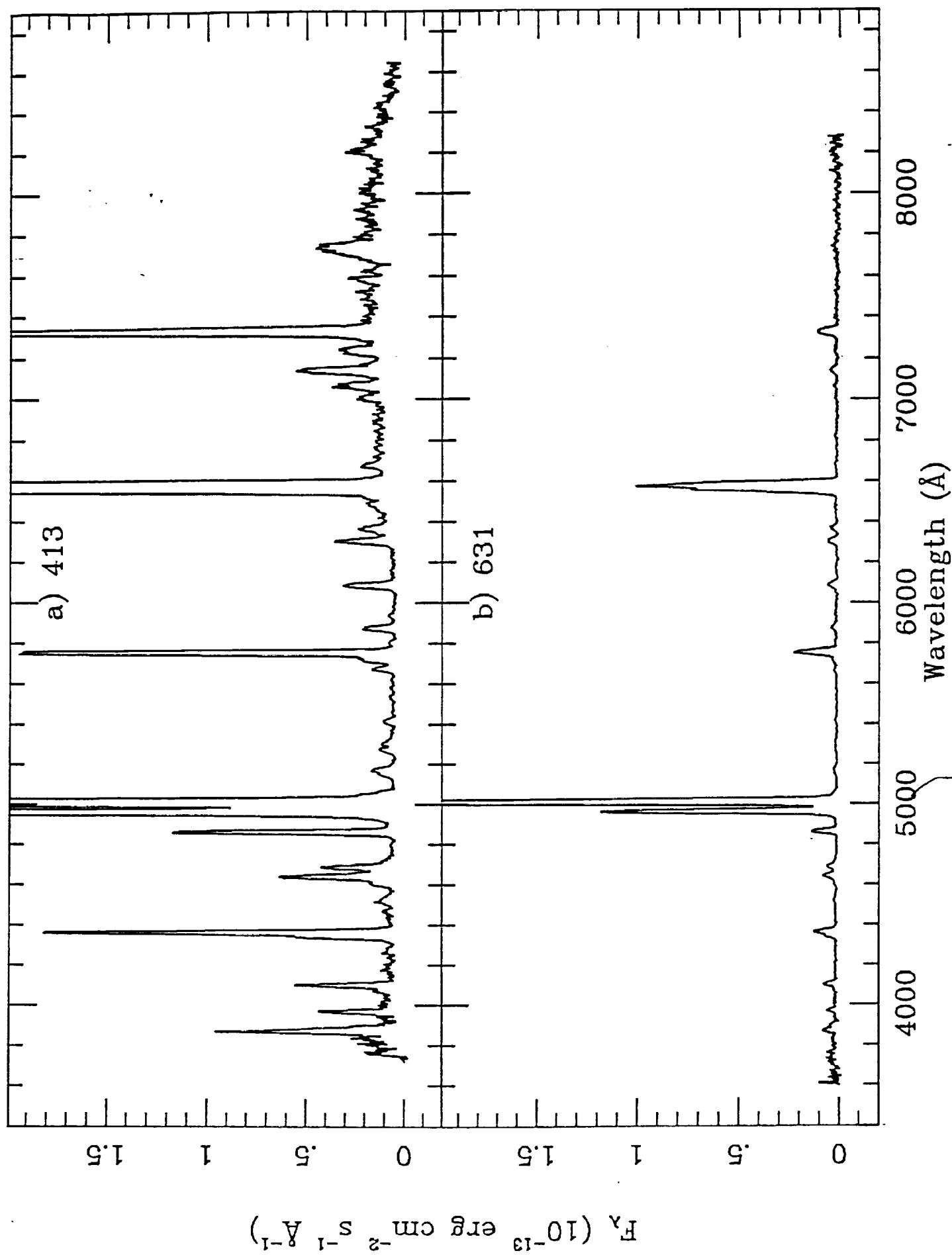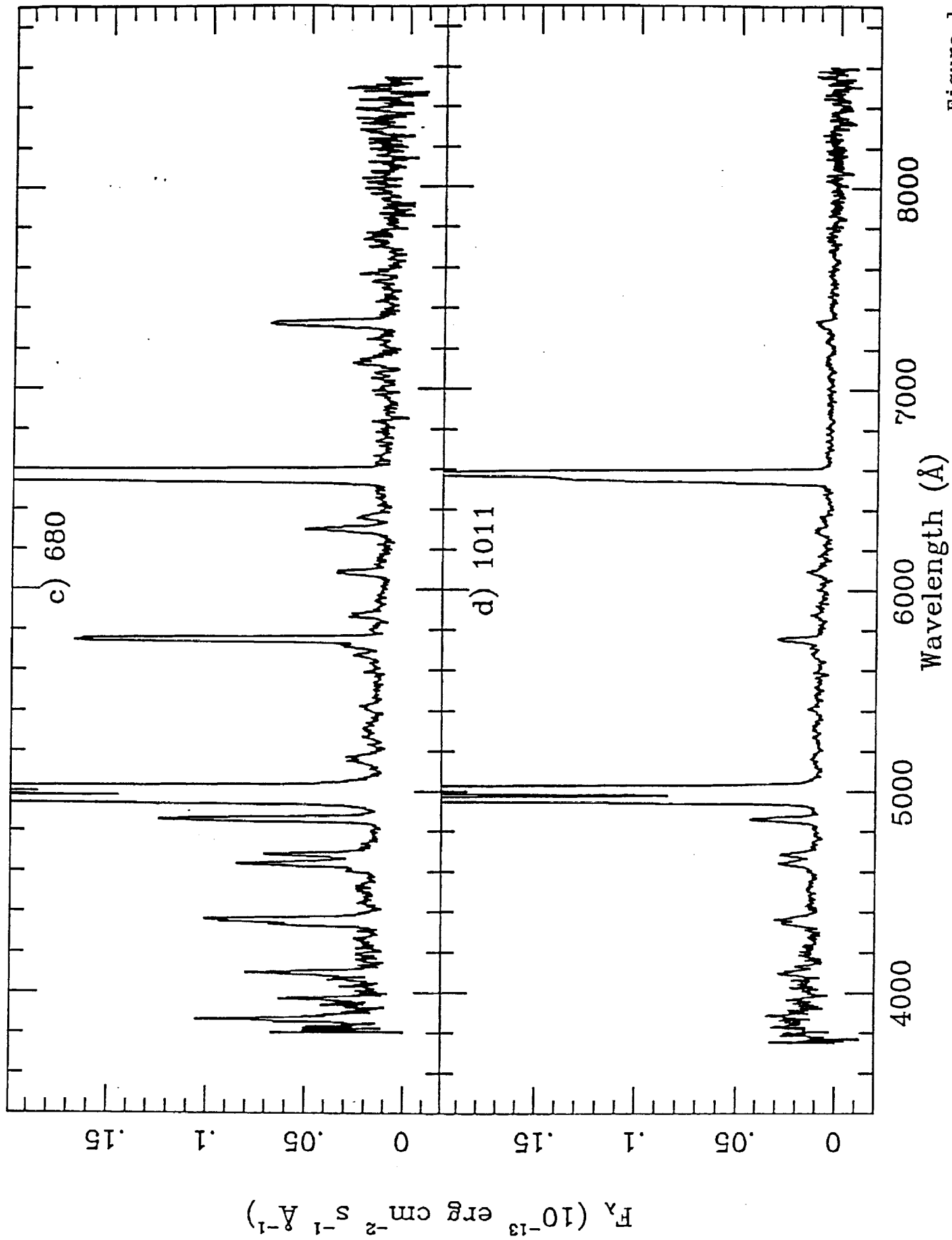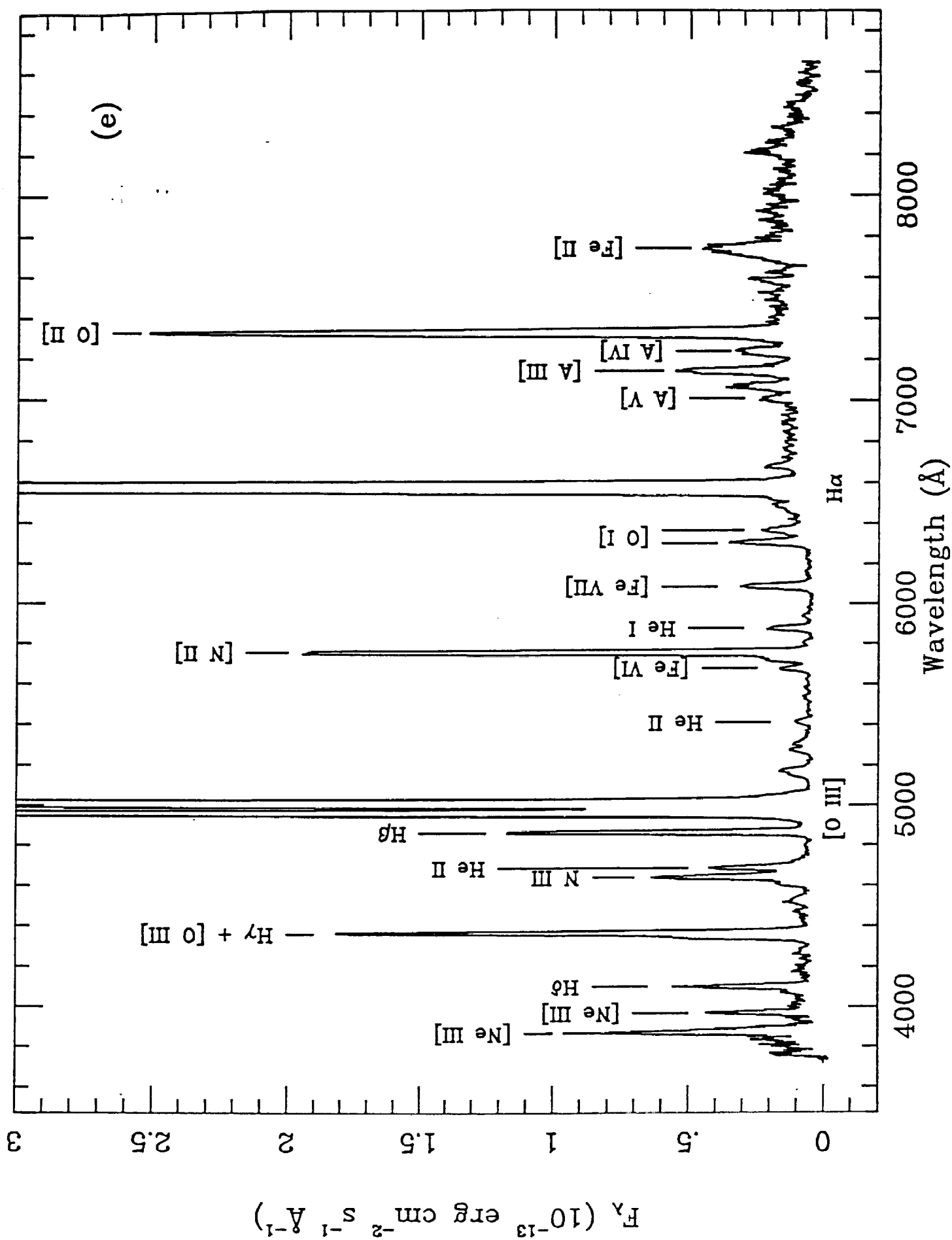
Figure 1

a) 413

b) 631

Wavelength (Å)

F_λ (10^{-13} erg cm^{-2} s^{-1} Å^{-1})

Figure 1

Figure 1

The figure shows a spectrum with the x-axis labeled "Wavelength (Å)" ranging from below 4000 to above 8000, and the y-axis labeled "F_λ (10^{-13} erg cm^{-2} s^{-1} Å^{-1})" ranging from 0 to 3.

Labeled emission lines include: [Ne III], [Ne III], Hδ, Hγ + [O III], Hβ, He II, N III, [O III], He II, [Fe VI], [N II], He I, [Fe VII], [O I], Hα, [A V], [A III], [A IV], [O II], [Fe II].

Panel label: (e)

(f)

Wavelength (Å)

Relative Intensity

Figure 2

F_λ (10^{-13} erg cm^{-2} s^{-1} Å^{-1})

Wavelength (Å)

a) 253

b) 331

Figure 2

e) 458

f) 611

Wavelength (Å)

F_λ (10^{-13} erg cm^{-2} s^{-1} Å^{-1})

Log t (days since outburst)

Log L(Hβ) (erg/sec)

[OIII]λ5007/Hβ

[OIII]λ4363/Hβ

Log R

Log t (days since outburst)

[OIII]λ5007/[OIII]λ4363

Log R

Log t (days since outburst)

Figure. Plot of Log Te versus Log Ne showing curves for [OIII]λ4363/[OIII]λ5007 (solid) and [OIII]λ1663/[OIII]λ5007 (dashed). Curves labeled "day 253" and "day 340".

Log [γ(ν)/4π j(Hβ)]

15.5   15   14.5   14   13.5

Log ν

−13   −14   −15   −16